Theoretical and Experimental Chemistry, Vol. 46, No. 2, 2010

SILVER AND GOLD NANOPARTICLES IN SILICA MATRICES: SYNTHESIS, PROPERTIES, AND APPLICATION

A. M. Eremenko, N. P. Smirnova, I. P. Mukha, and H. R. Yashan

UDC 661.682:544.7:544.52:546.57/59

Methods of synthesis, optical characteristics, morphology, and catalytic and bactericidal characteristics of composite materials based on silica (films and powders) containing nanoparticles of silver, gold, and their binary compounds with alloy or core–shell structure are examined. The photochemical reduction of Au^{3+} and Ag^{+} with a photocatalyst (a film of SiO_2 with adsorbed benzophenone) makes it possible to generate stable nanoparticles of gold and silver in solutions for subsequent introduction into adsorbents and catalysts. Examples of the use of nanosized composites in catalysis and in microbiological experiments are presented.

***Key words**: nanoparticles, gold, silver, photoreduction, optical spectra, structure of nanoparticles, sol–gel process, bactericidal properties.*

INTRODUCTION

The production and properties of nanosized clusters and the nanoparticles of metals (Me NP) was and remains an extremely active field of research in connection with the enormous prospects for their use in optics, optoelectronics, catalysis, medicine, etc. [1-6]. The nanoparticles of noble metals Au and Ag exhibit unusual optical, electric, and magnetic characteristics, which distinguish them both from the bulk metal and individual atom or ion properties. One of the most interesting aspects of the metal nanoparticles is the strong dependence of their optical properties, namely color, on the size and shape of the particles. Gold nanoparticles have a visible color that varies from yellow to blue through all shades of red. This effect results from change of the so-called surface plasmon resonance (SPR), the frequency at which the conduction electrons oscillate in response to change in the electric field of the incident electromagnetic radiation. Only metals with free electrons (Ag, Au, Cu, and alkali metals) exhibit SPR in the visible region, displaying intense colors. The electric field of the incident radiation initiates the formation of a dipole in the nanoparticles. The reciprocal force in the nanoparticles compensates for it, leading to an unique resonance of the wavelength [7].

The nanoparticles of the metals are produced by various methods, the most popular of which are the photochemical or radiation-chemical methods in the presence of sensitizers: sodium tetrahydroborate, hydrazine, glucose, sodium citrate, etc. [8-10]. The reduction of the ions to metal nanoparticles in solid matrices takes place under appropriate conditions as a result of sonochemical deposition, thermal action, laser ablation on a substrate, and other methods [11-21]. Organic solvents such as ethanol, ethylene glycol, and isopropyl alcohol have also been used as reducing agents for the production of nanoparticles of colloidal gold and silver from aqueous solutions of $AgNO_3$ and $HAuCl_4$ in the presence of protective components such as polyvinylpyrrolidone (PVP), surfactants, polyols [22-25], and amphiphilic block copolymers [26]. The addition of

O. O. Chuiko Institute of Surface Chemistry, National Academy of Sciences of Ukraine, Vul. Generala Naumova, 17, Kyiv 03164, Ukraine. E-mail: annaerem@ukr.net. Translated from Teoreticheskaya i Éksperimental'naya Khimiya, Vol. 46, No. 2, pp. 67-86, March-April, 2010. Original article submitted February 23, 2010.

benzophenone (BP) to the reaction mixture leads to an increase in the rate of photoreduction of the metal ions and sensitizes the reaction to near UV radiation (355-365 nm) [27]. Earlier we demonstrated the effectiveness of silica modified with BP molecules as photocatalyst for the reduction of silver, gold, palladium, and chromium ions in solutions and in heterogeneous systems [28-31].

Interaction of the Nanoparticles of Noble Metals with Solvents, Surfactants, and Oxygen

In order to understand the optical effects in solutions of the nanoparticles of noble metals it is important to know the nature of the chemical and physical interactions of the nanoparticles with the surroundings. Solvate interaction of the solvent molecules with nanoparticles occurs as a result of van der Waals forces and is weak [32-34].

In [35] the effect of various solvents on the position of the SPR band in sols of gold nanoparticles of diameter 6 nm was analyzed. In the change of water to acetonitrile with increase of the refractive index the absorption maximum of the SPR band of the nanoparticles is shifted toward the red region from 520 to 532 nm. The shift of the SPR band depends not so much on the refractive index as on the donor capacity of the molecules capable of complexation with the gold nanoparticles, the atoms of which are coordinationally unsaturated. The molecules of nucleophiles are able to give up their electron density to the free orbitals of the gold atoms by direct organic ligand → Au nanoparticle charge transfer [36, 37].

Hydrophilic–hydrophobic interaction arises between the molecules of the cationic and anionic surfactants and the nanoparticles of the metal, and as a result a dense dielectric shell appears around the nanoparticles, the electric field becomes nonuniform, and the SPR band undergoes a bathochromic shift. In the presence of a group capable of specific interaction with the surface of the Au or Ag nanoparticles (e.g., —OH, —NH_2, —SH) it is chemisorbed on the surface, and the ligands here draw excess electron density from the surface of the nanoparticles [32]. Aliphatic alcohols cause minimal displacement and thiols maximal one [35]. During contact between the silver nanoparticles and oxygen [34] the intensity of the plasmon peak decreases substantially, and the SPR band undergoes a bathochromic shift. Under the same conditions the spectrum of the gold nanoparticles remains practically unchanged [35]. The surface of the silver nanoparticles is oxidized by oxygen dissolved in the water. X-ray spectral analysis does not reveal oxide structures on the surface, but they can be seen in the X-ray photoelectron spectra [38]. Decrease of the electron density on the surface of the nanoparticles is accompanied by their coagulation and aggregation, i.e., the sols of the nanoparticles are unstable.

Production and Properties of Nanoparticles in Heterogeneous Oxide Systems

A new class of materials based on nanoparticles in the composition of semiconductors (TiO_2, ZnO, etc.) and dielectrics (SiO_2, Al_2O_3, etc.) substantially extends the range of their application, particularly in heterogeneous catalysis, in the creation of electronic devices, chemical sensors, protecting coatings, bactericidal materials, for surface enhanced Raman scattering, etc. [39-41]. It is fundamentally important in this connection to develop methods for the synthesis of systems based on NP/MeO and to investigate the nature of the interaction of nanosized particles with the oxide matrix. In the present work greatest attention is paid to the production and characteristics of nanoparticles in silica films and powders. The stability, optical characteristics, and morphology of the nanoparticles in silica are determined by the method of production, the degree of dispersion, the presence of pores, the heat treatment regime of the SiO_2, and the method of introduction of the metal nanoparticles into the solid matrix. Methods for the deposition of silver nanoparticles on the surface of silica, involving the use of nonionic inverse micelles, have been described in the literature [11]. The sol–gel method supposes mutual gelation of the silica with a metal salt during hydrolysis and polycondensation of tetraethoxysilane (TEOS) followed by reduction of the ions to nanoparticles [12, 13]. The metal nanoparticles are located in the pores and are accessible to the molecules of the reactants. Uniform distribution of the silver clusters in the mesopores of the SiO_2 monolith was achieved by impregnation the silica with silver nitrate followed by reduction in a stream of hydrogen [14]. Sonochemical deposition of the gold nanoparticles into the pores of silica [15] and of silver onto the surface of submicrospherical SiO_2 [16] has been used to create structures of the metallic shell–SiO_2 core type. The authors of [17] investigated the thermal stability of silver nanoparticles on spherical particles of SiO_2 and the change of their form during heat treatment – from hemispherical at 350-550 °C to spherical on heating to 550-700 °C as a result of

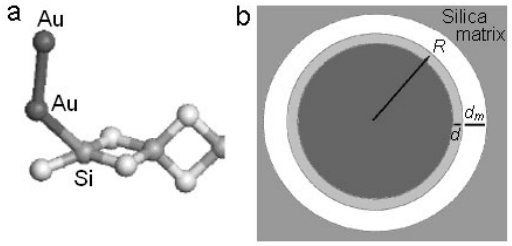

Fig. 1. a) Model of the bonding of the metal atom with the coordination unsaturated silicon atom according to [42]. b) Localization of the metal nanoparticle in the pore of silica – the core–shell model according to [58].

diffusion and the beginning fusion of the metal nanoparticles. After 750 °C the spherical silver nanoparticles crumbled from the surface of the silica as a result of decrease in the area of contact and the bonding forces between the nanoparticles and the substrate.

From analysis of the published data it is possible to reach a conclusion about several models of the localization of the metal nanoparticles in the silica matrix. In principle, the metals are weakly bonded to the surface of the SiO_2, but the presence of defect centers and oxygen vacancies leads to interaction of the metal atom with a small cluster of silica through such unsaturated bonds. In the presence of gold atoms in the system the coordination bonds of the silicon are saturated to CN = 4, as demonstrated by means of the theory of the density distribution of the probability of atomic orbitals in [42]. The adsorbed metal atoms in turn act as centers (nuclei) for growth of Au islands (Fig. 1a) [43-48]. According to [49], the nucleation and subsequent growth of gold clusters on a SiO_2 film take place by way of a decrease of stability on the complexes in the order oxygen vacancies > linear defects > single oxygen vacancies. Moreover, the defect centers can change the chemical and electronic characteristics of the deposited metal particles as a result of the charge transfer between the substrate and the metal cluster [50, 51]. The bond between the Ag and SiO_2 is covalent and does not depend on the concentration of the defects. With small amounts the silver nanoparticles grow as 2D structures, and if the degree of coverage is increased 3D structures are formed [52]. The authors discuss the formation of covalent bonds between the silver nanoparticles and the defect centers of the SiO_2 film during their investigation by metastable pulse electronic spectroscopy and ultraviolet photoelectron spectroscopy. The silver clusters carry a positive charge as a result of electron transfer from the Ag to the SiO_2 with partial reduction of the Si(IV) [53]. The analogous situation for gold was discussed in [54]. Interaction between the gold nanoparticles and the walls of the pores in the silica reduces the surface energy of the system. The Au—Si bonds that form (on account of electron transfer from the Au to the SiO_2) reduce the density of free electrons close to the surface of the gold particles. It was found by X-ray photoelectron spectroscopy (XPS) that the spin doublet Au4*f* (Au4$f_{5/2}$ 86.6 eV and Au4$f_{7/2}$ 83.3 eV) is shifted toward lower bonding energies compared with the standard values for the metal (87.4 eV for 4$f_{5/2}$ and 83.8 eV for 4$f_{7/2}$). This corresponds to relatively strong interaction in the metal–substrate system.

The selective reduction and the separate distribution of the gold and silver nanoparticles in silicate glasses under the influence of femtosecond laser irradiation followed by heat treatment were reported by the authors of [55]. The coverage of the metal nanoparticles by a shell of silica makes it possible to vary widely the degree of dispersion of the nanoparticles in solvents with various polarities and to produce materials of the silica shell–polydispersed metal core type with controllable particle shape [56]. An approach to the production of nanoparticles covered with a silica shell using an amphiphilic nonionic polymer of PVP as binding agent between the metal nanoparticles and the silica was described in [57]. A two-layer core–shell model with the metal in a pore in the silica, separated from the SiO_2 matrix, is shown in Fig. 1b, where R is the radius of the metal nanoparticle (core), *d* is the thickness of the silica shell, and d_m is the thickness of the "cavity" around the core–shell structure [58].

The authors of [59] maintain that in an electric field of constant current the state of aggregation of the silver atoms varies and at the nanoparticle–SiO_2 boundary there is a chemical reaction leading to the formation of a bond between the

nanoparticle and the silicon and the formation of an oxide phase around the nanoparticle: $Ag + SiO_2 \rightarrow AgSi + O_2$; $2Ag + SiO_2 \rightarrow Si + 2AgO$.

The Properties of Bimetallic Ag/Au Nanoparticles in Silica Matrices

One of the recently appearing and actively developed trends in the creation of new prospective materials is the synthesis of composite bimetallic nanoparticles (BMNP), in which two metals coexist. The electronic spectra, the structure of the BMNP, the chemical stability, the optical characteristics, their activity in various biological processes, and the selectivity in catalytic reactions differ greatly from the properties characteristic of the individual metals [6, 60-64].

The transition from mono- to bimetallic particles is accompanied by a change in the energy of surface plasmon absorption depends on the components of bimetallic composition. The bimetallic nanoparticles consisting of gold and silver are of great practical significance in optoelectronics, catalysis, medicine, biology (as biosensors), etc. In many publications the production of bimetallic nanoparticles in the form of layers, core–shell composites, alloys, nanotubes, etc. has been reported [62, 65-67].

The properties of bimetallic nanoparticles are regulated by such parameters as the size and shape of the nanoparticles, the ratio of the components, the order in which they crystallize, and the stabilization and ordering of the nanocrystals [68-73]. The methods for the production of the nanoparticles of the individual metals and of the bimetallic nanoparticles are similar: photoreduction, chemical reduction in aqueous media in the presence of stabilizers (polymers, inverse micelles), thermal reduction [30, 74-90]. There is no doubt that the photochemical method for the reduction of nanoparticles and bimetallic nanoparticles from their ions is the most economical and energy- and time-saving in comparison with other methods [29-31, 77].

Thus, in spite of the enormous number of publications on the synthesis of nanosized metallic particles in solid-state oxide matrices the detailed processes occurring between the oxides and metals, particularly between Ag and Au nanoparticles and SiO_2, are far from clear. This concerns, in particular, the question of the distribution of the nanoparticles over the surface and the volume of the films and in the silica powders, irrespective of the method of production, their morphology, crystallinity, stability, and susceptibility to aggregation. A complex matter is the question of the production of bimetallic nanoparticles with a given morphology in the composition of the silica film, taking account of their various electrochemical reduction potentials ($Ag^+/Ag_{atom} = -1.8$ V, $Au^{3+}/Au_{atom} = -1.5$ V) [78] and also the stabilization of the silver nanoparticles on the surface of dispersed silica as a result of its susceptibility to oxidation. Also important is the development of a method for the production of bimetallic nanoparticles in which the formation of an insoluble precipitate of silver chloride in the presence of tetrachloroauric acid during their reduction is prevented. Of fundamental and applied interest is investigation of the accessibility of the nanoparticles in the silica composite for the reagent molecules, their effect on the photostability of the admolecules, and their role in the processes of photocatalytic decomposition of the contaminant molecules from the environment.

In the present work we will dwell briefly on analysis of results dedicated to some of the questions enumerated above obtained in the department of surface photonics at the O. O. Chuiko Institute of Surface Chemistry, National Academy of Sciences of Ukraine.

PHOTOCATALYTIC PRODUCTION OF Ag AND Au NANOPARTICLES IN WATER–ALCOHOL SOLUTIONS AND ON THE SURFACE OF MESOPOROUS SILICA

As mentioned above, the presence of benzophenone in the reaction mixture leads to an increase in the rate of photoreduction of the metal ions and sensitizes the reaction to near UV radiation (355-365 nm) [27]. This photochemical reaction formed the basis of the creation of the effective photocatalyst BP/SiO_2 (BP adsorbed on the surface of porous films and powders of silica) for the reduction of the ions of noble metals in colloidal solutions and in solid matrices, in particular SiO_2. The BP molecules adsorbed on the surface of silica are accessible to the metal ions present in the solution. It is known that the adsorption of ketones on silica at low degrees of coverage takes place on account of the formation of hydrogen bonds between

the C=O and the two silanol (vicinal ≡Si—OH) groups [79]. It was established that BP adsorbed on silica gel at a level not exceeding 8.4% of a monolayer is hardly desorbed at all in hexane solution (not more than 0.6-1% of the total amount of adsorbed molecules) [31, 80]. It is much more convenient to use films of silica than dispersed SiO_2 as photocatalysts for the production of nanoparticles of metals on account of the absence of the filtration stage; films with an ordered mesostructure were therefore synthesized by the sol–gel technique by the hydrolysis of tetraethoxysilane 98% (TEOS) using the nonionic triblock copolymer Pluronic P123 or the cationic surfactant cetyltrimethylammonium bromide (CTAB) as pore creating agent.

The Sol–Gel Procedure for the Production of Silica Films

The sol–gel procedure for the production of silica films was described in [81]. Briefly the synthesis consisted of the following. After hydrolysis of TEOS for 24 h an aqueous solution of CTAB was added to the mixture. The molar ratios of the components of the precursor were: 1TEOS : 0.1CTAB : 0.02HCl : $10H_2O$: $5C_2H_5OH$. The films of SiO_2 were deposited on glass substrates by vertical drawing from the precursor (the dip-coating technique). They were then dried in air for 12 h followed by heating to 400 °C at a rate of 1 deg/min and holding at 400 °C for 6 h. After treatment the surface area of such films amounted to 600-650 m^2/g.

Production of Photocatalyst for the Reduction of Silver and Gold Ions

Silica films and powders form the basis of the production of the photocatalyst BP/SiO_2. The adsorption of BP on dispersed silica gel (SG) Davisil SG-150Å with specific surface area 300 m^2/g was realized from a $3\cdot10^{-3}$ M solution of BP in hexane, and adsorption on mesoporous films of SiO_2 was realized from a $3\cdot10^{-4}$ M solution of BP. The amount of adsorbed BP was ~$1\cdot10^{-4}$ mol/g in the case of SG and ~$2\cdot10^{-4}$ mol/g in the case of the SiO_2 films, i.e., 4% of the volume of the monolayer.

Production of Silver and Gold Nanoparticles in Colloidal Solutions

Mesoporous silica films and powders modified with benzophenone were investigated as photocatalysts for the reduction of silver and gold ions in aqueous solution [28-31]. A DRSh-500 high-pressure mercury lamp with a UV 7-60 filter was used as light source with wavelength 365 nm. The band with wavelength 253.7 nm was isolated from the spectrum of a PRK-1000 mercury lamp with a standard chemical light filter ($CoSO_4\cdot7H_2O$ 8.4 g/100 mL of H_2O). The choice of irradiation wavelengths was based on the absorption region of the BP molecules. The reaction vessel was a quartz cylinder of volume 25 mL. The intensity of the incident light with wavelengths 253.7 and 365 nm, determined with potassium tris(oxalato)ferrate(III) as actinometer [88], amounted to $2\cdot10^{17}$ and $3.3\cdot10^{16}$ quanta/s·cm^2 respectively. The solution was irradiated in an atmosphere of argon. The absorption spectra of the solutions before and after irradiation were measured in a quartz cuvette with a thickness of 1 cm on a Perkin Elmer Lambda UV-Vis spectrometer. The diffuse reflection spectra of the powders were measured on the same spectrometer using a sphere.

The Mechanism of Reduction of Ag and Au Ions and Formation of Nanoparticles of the Metals

During irradiation with light with $\lambda = 253.7$ and 365 nm the BP molecule changes into the excited reactive triplet state, which is capable of abstracting a hydrogen atom from aliphatic alcohols, and two ketyl radicals are formed. The latter undergo protolytic dissociation with the formation of radical-anions of BP and isopropyl alcohol, having large electrochemical potentials and capable of reducing the ions of the noble metals [34]. The electrochemical potential of silver is more negative than that of such ketyl radical of isopropyl alcohol but less negative than for the corresponding radical-anions; it is, therefore, probably the BP radical-anions that are active in the photoreduction of the silver ions, and this agrees with the proposal put forward by Henglein [83].

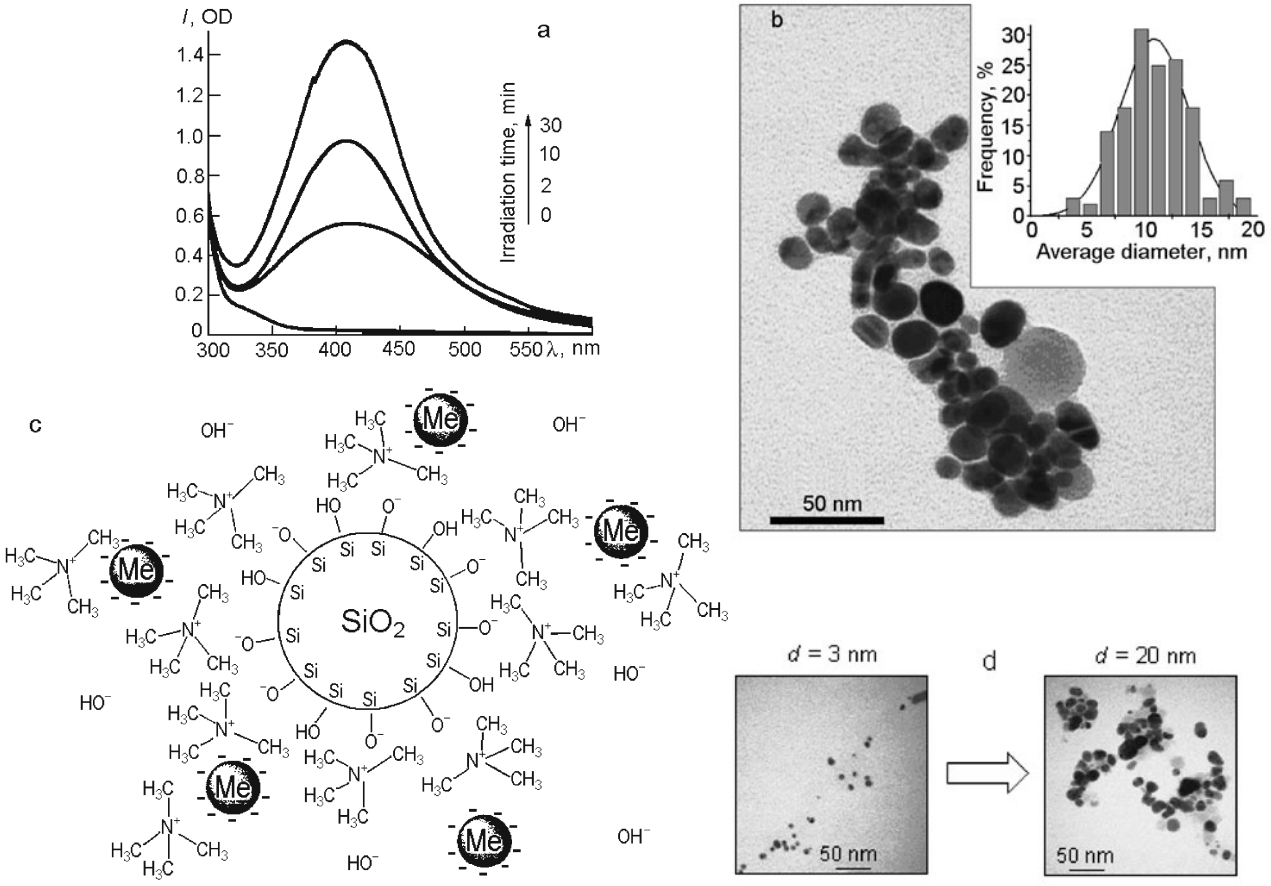

Fig. 2. a) The evolution of the absorption spectra of Ag nanoparticles stabilized with Ludox in solution with irradiation time in the presence of BP/SiO_2 [C(BP) = $2.83 \cdot 10^{-5}$ mol/g]. b) The TEM of Ag nanoparticles on the surface of the stabilizer Ludox (the gray spheres are the stabilizer particles, the dark spheres are the Ag nanoparticles); the inset shows the size distribution of the particles. c) Model of the adsorption of the metal nanoparticles on the surface of the Ludox particle. d) Variation of the diameter of the Ag nanoparticles with time.

Photogeneration of Silver Nanoparticles in Solutions

Stable nanosized silver colloids were produced during the irradiation of $AgNO_3$ solution in the presence of BP/SiO_2 mesoporous powders and films. Sodium dodecyl sulfate (SDS) or the stable colloidal silica Ludox was used as stabilizer during the photochemical formation of nanosized silver in solution [28].

Irradiation of the BP/SiO_2–Ag^+ system with light having $\lambda = 253.7$ nm in the presence of Ludox leads to the appearance of a SPR band with a characteristic maximum at 390-410 nm in the absorption spectrum (Fig. 2a). From measurement of the kinetics of the process, determined from the dependence of the intensity of the maximum of the SPR band at $\lambda = 407$ nm on the irradiation time, it follows that the reaction during irradiation takes place three times faster in the presence of the BP/SiO_2 films than in the absence of the photocatalyst. The quantum yield was 18.2%. The silver nanoparticles in solution are not in the free state but in the form of clusters on the surface of the spherical particles of colloidal silica stabilized by the quaternary ammonium base TMAOH (Fig. 2b). The reason for such behavior may be the fact that the first-reduced Ag atoms are adsorbed on the surface of the stabilizer – colloidal SiO_2, as shown in Fig. 2c, forming centers for the growth of the metal nanoparticles. The diameter of such nanoparticles varies in the range between 3 and 20 nm (Fig. 2d).

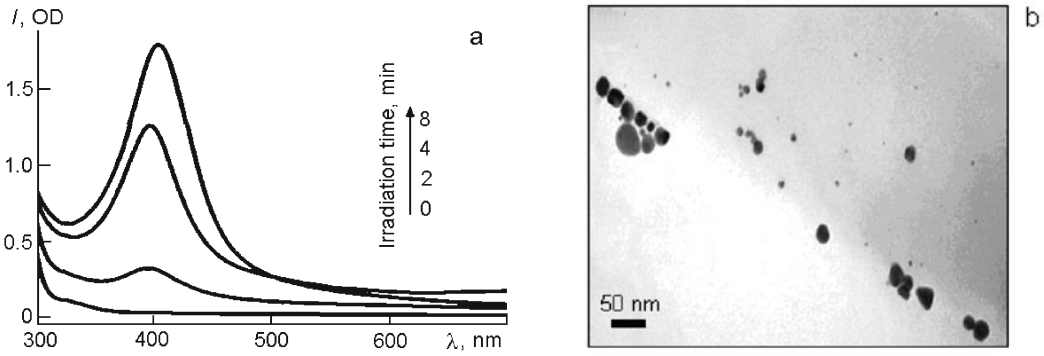

Fig. 3. a) The evolution of the absorption spectra of silver nanoparticles in solution with irradiation time of Ag^+ in the presence of BP/SiO_2, $C(BP) = 2.83 \cdot 10^{-5}$ mol/g. b) The TEM of silver nanoparticles stabilized with SDS.

If SDS is used as stabilizer small aggregates of nanoparticles (clusters from 2-10 nanoparticles) are formed in addition to the non-aggregated particles, and here the SPR band is narrower while the position of its maximum is shifted a little toward the long-wave part of the spectrum (Fig. 3).

In general the scheme for the photogeneration of silver nanoparticles in the presence of BP/SiO_2 in solution in isopropyl alcohol (IPA) can be represented in the following form:

1) The formation of the triplet state of BP during the action of a quantum of light:

$$(C_6H_5)_2C{=}O \xrightarrow{h\nu} (C_6H_5)_2C{=}O^*.$$

2) Abstraction of a hydrogen atom from the IPA molecule and formation of two ketyl radicals:

$$(C_6H_5)_2C{=}O^* + (CH_3)_2CHOH \rightarrow (C_6H_5)_2C^{\cdot}OH + (CH_3)_2C^{\cdot}OH,$$

$$(C_6H_5)_2C{=}O + (CH_3)_2C^{\cdot}OH \rightarrow (C_6H_5)_2C^{\cdot}OH + (CH_3)_2C{=}O,$$

3) Protolytic dissociation of the ketyl radicals:

$$R_2C^{\cdot}OH \rightarrow R_2C^{\cdot}O^- + H^+ \ (R = CH_3, C_6H_5),$$

4) Reduction of the silver ions by the ketyl radical-anions:

$$R_2C^{\cdot}O^- + Ag^+ \rightarrow R_2C{=}O + Ag,$$

5) Formation of silver nanoparticles:

$$n\mathrm{Ag} \rightarrow (\mathrm{Ag})_n,$$

6) Peptization of the Ag nanoparticles by the ketyl radical of BP:

$$(C_6H_5)_2C^{\cdot}OH + (Ag^0)_n \rightarrow (C_6H_5)_2CO + (Ag^0)_n^- + H^+,$$

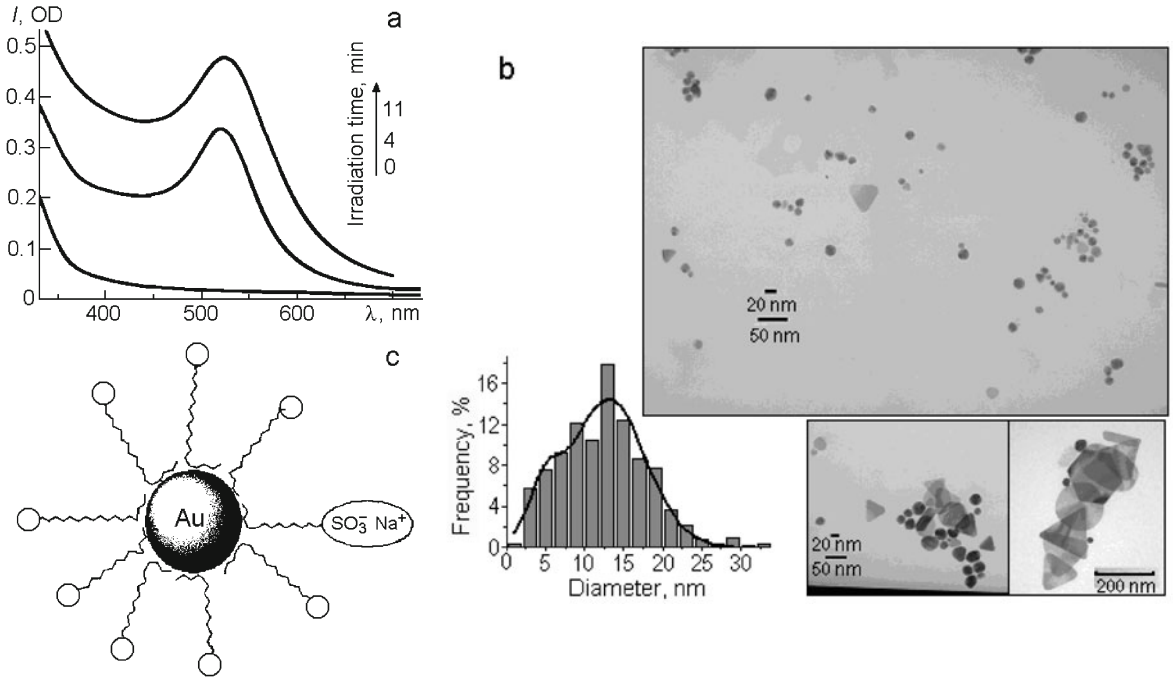

Fig. 4. a) The evolution of the absorption spectra of Au nanoparticles with the irradiation time of a solution of $HAuCl_4$ in the presence of BP/SiO_2; nanoparticles stabilized with SDS. b) The TEM of the gold nanoparticles in the colloidal solution; the inset shows the size distribution of the particles and the aggregation of the nanoparticles during maturation. c) Model of the stabilization of the Au nanoparticles in SDS micelles.

$$(Ag^0)_n^- + Ag^+ \rightarrow (Ag^0)_{n+1}.$$

Photogeneration of Au Nanoparticles in Solutions

Irradiation of the BP/SiO_2–$AuCl_4^-$ systems in the presence of SDS as stabilizer leads to the appearance of the SPR band of nanosized gold with a characteristic maximum at 520-530 nm in the absorption spectrum of the solution (Fig. 4a). The absorption coefficient of colloidal gold obtained by means of the Bouguer–Lambert–Beer equation $\varepsilon = 3.33 \cdot 10^3$ $M^{-1} \cdot cm^{-1}$ at $\lambda =$ 520 nm agrees well with published data $\varepsilon = 3.2 \cdot 10^3$ $M^{-1} \cdot cm^{-1}$ [84].

The calculated yields amount to 5.5% for the photoreduction of gold ions in the presence of the photocatalyst and 0.6% in the control experiment [30].

From the instant absorption spectra of the products from the photoreaction of BP with isopropyl alcohol [85] and our previously obtained emission and excitation spectra of BP [80] it is possible to confirm a similar mechanism for the photogeneration of silver and gold nanoparticles with the participation of BP in the triplet state, producing as a result of protolytic dissociation in a weak alkaline medium the radical-anions of BP and isopropyl alcohol [35], which have an electrochemical potential sufficient for the reduction of Au^{m+} ($E^0_{Au^{3+}/Au^{2+}} > +1.29$ V, $E^0_{Au^+/Au^0} = -1.47$ V).

We suppose that the main contribution to the photocatalytic reduction of the silver and gold ions in the presence of BP/SiO_2 comes from the ketyl radicals and the radical-anions of isopropyl alcohol, initiated by BP in the triplet state, since the bulk of them exist in the solution unlike the BP radicals attached to the surface of the SiO_2. The generation and growth of the gold nanoparticles occur simultaneously, and the latter begins to predominate when the concentration of tetrachloroaurate ions becomes smaller than the concentration of the initial nanoclusters. The ketyl radicals of isopropyl alcohol are capable

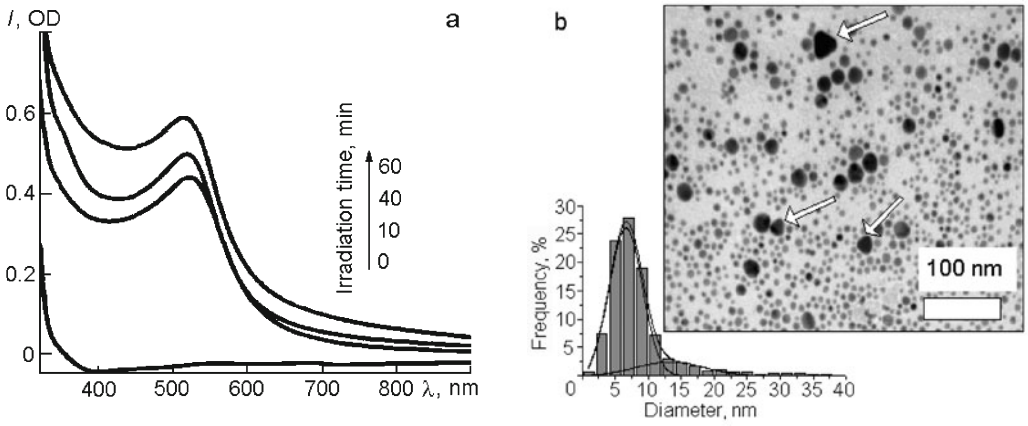

Fig. 5. a) The evolution of the absorption spectra of a colloidal solution of bimetallic Ag/Au nanoparticles (alloy) during irradiation (Me ions added to reaction vessel simultaneously in a ratio of Ag : Au = 1 : 1). b) The TEM of this sample; inset, BMNP size distribution.

interacting with the surface atoms of the Au nanoparticle, giving up one electron, by analogy with [34], and here negative charge accumulates on the particle:

$$k(CH_3)_2C^{\cdot}—OH + Au_n \rightarrow Au_n^{k-} + kH^+ + k(CH_3)_2CO.$$

Further reduction of the gold ions takes place on the surface of the negatively charged nanoparticle:

$$Au_n^{k-} + Au^{m+} \rightarrow Au_n^{(k-m)-}.$$

The growth of the Au nanoparticles is realized in this way.

The gold particles produced in the presence of SDS are not aggregated, the fine particles have spherical form, and the coarse particles have the form of a trigonal prism. In solution the fine particles form aggregates as a result of coagulation in the maturation process. On the transmission electron micrograph (TEM) of the gold nanoparticles in colloidal solution there are aggregates consisting of Au nanoparticles in the form of prisms, tubes, and spheres (Fig. 4b, c).

Production of Ag/Au Bimetallic Nanoparticles in Colloidal Solutions

Colloidal solutions of the bimetallic nanoparticles were produced during successive or simultaneous irradiation of solutions of $HAuCl_4$ and $AgNO_3$ in the presence of the photocatalyst BP/SiO_2 in water–IPA solution. Sodium dodecyl sulfate and cetyltrimethylammonium bromide were used as stabilizers during the synthesis of the nanoparticles of the noble metals; their concentrations in the solutions were $4.5 \cdot 10^{-4}$ M. Colloidal silica (Ludox) at a concentration of up to 1 vol.% in the reaction mixture was also used to stabilize the nanoparticles.

Ag/Au Bimetallic Nanoparticles with Alloy Structure

Metallic nanoparticles of the alloy type were formed by UV irradiation of a solution containing gold and silver ions. One absorption maximum was observed during their simultaneous reduction (Fig. 5a).

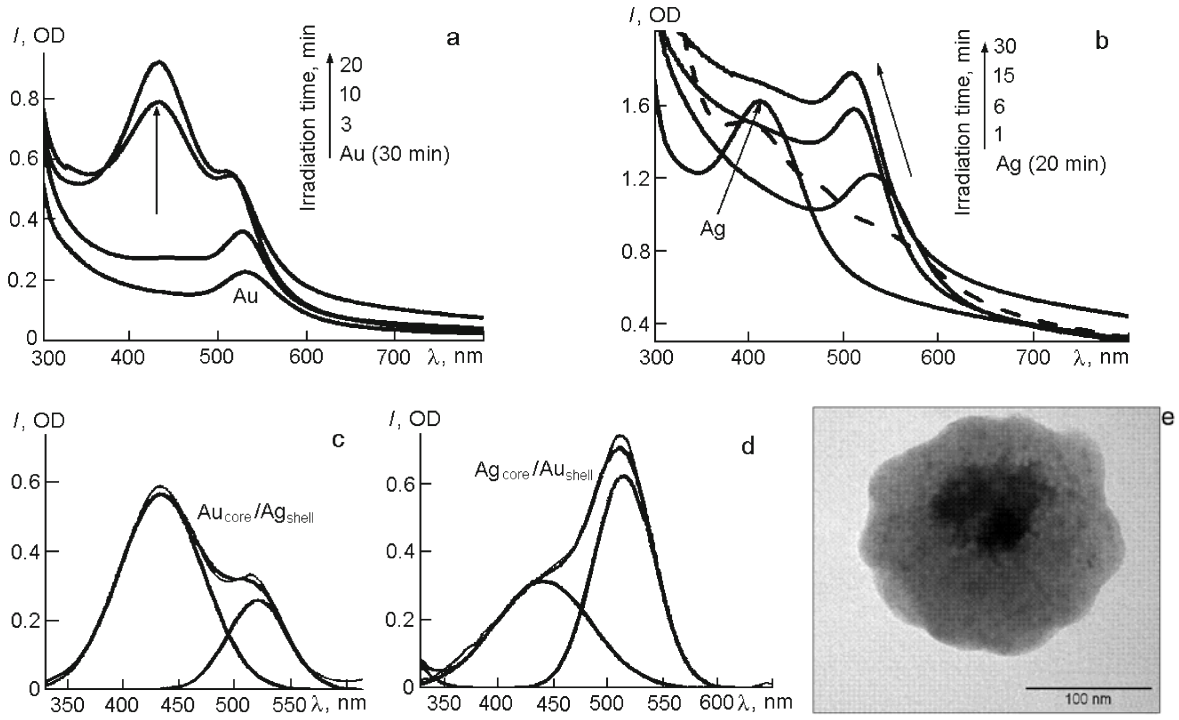

Fig. 6. a), b) The evolution of the absorption spectra of colloidal solutions of bimetallic nanoparticles Au_{core}/Ag_{shell} (a) and Ag_{core}/Au_{shell} (b) with the irradiation time with the ratio Ag : Au = 1 : 1. c), d) Expansion of the final normalized spectrum in Gaussian approximation for Au_{core}/Ag_{shell} (c) and Ag_{core}/Au_{shell} (d) nanoparticles. e) Transmission electron micrograph of Au_{core}/Ag_{shell} nanoparticles in colloidal solution.

The intensity of the maximum increases with the irradiation time of the solution. The size of the particles lies in the range of 2.5-10 nm, and the maximum of the SPR band is shifted toward the side of the absorption of the gold nanoparticles. It is seen from the transmission electron micrograph (Fig. 5b) that in addition to the spherical bimetallic nanoparticles of the alloy there are individual nanoparticles of gold (shown by the arrows) in the form of triangular prisms, which explains the shift of the SPR maximum toward the characteristic value for gold nanoparticles. The reason for such an effect may lie in the non-stoichiometry of the formed alloy with a preponderance of silver in the bimetallic nanoparticles.

Ag/Au Bimetallic Nanoparticles with Core–Shell Structure

During the successive reduction of the ions in solution, for example, gold nanoparticles are formed initially, and then during the addition of silver ions the Au_{core}/Ag_{shell} structure is formed (Fig. 6a, c, e). During irradiation of the ions in solution in reverse order the Ag_{core}/Au_{shell} structure is formed. In the absorption spectrum the dominant absorption maximum characteristic of gold is clearly seen together with the absorption band of the silver nanoparticles, which form the core of this structure (Fig. 6b, d). Immediately after the addition of tetrachloroauric acid to the colloidal solution of Ag nanoparticles three maxima appear in the absorption spectrum: at 400, 475, and 547 nm. With time the first two maxima disappear, while the third one increases in proportion to the increase of the irradiation time and is shifted somewhat toward the shortwave region, which may indicate diffusion of the silver nanoparticles into the gold shell as a result of the almost identical lattice constants. The dashed line in Fig. 6b shows the intermediate stage of formation of the Ag/Au core–shell structure.

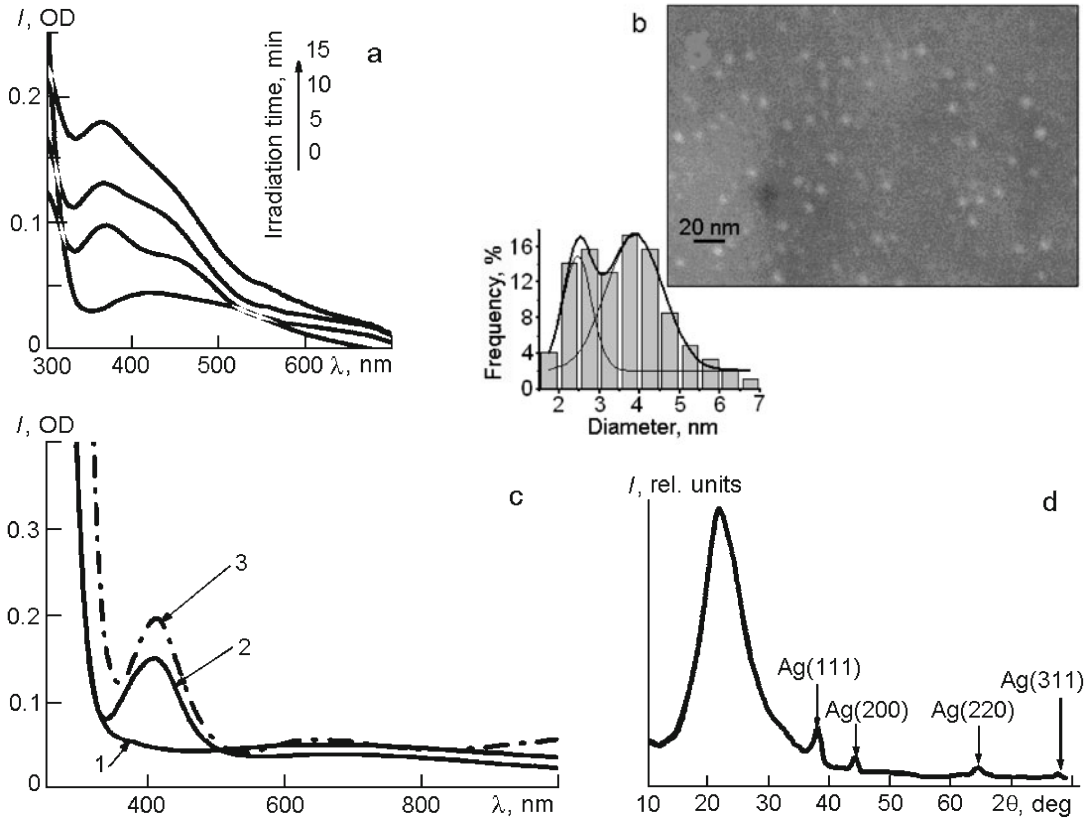

Fig. 7. a) The evolution of the absorption spectra of Ag nanoparticles in a film of SiO_2 with the irradiation time in a 10^{-3} M solution of BP in isopropyl alcohol. b) The SEM image of the Ag/SiO_2 film after irradiation for 15 min. c) The absorption spectra of Ag/SiO_2 films (2% Ag) before (1) and after (2) irradiation for 15 min in a $1.4 \cdot 10^{-3}$ M solution of benzophenone in isopropyl alcohol and the spectrum of the Ag/SiO_2 film after treatment at 500 °C for 6 h (3). d) The X-ray spectrum of the Ag/SiO_2 film.

PHOTOGENERATION OF Ag, Au, AND BIMETALLIC NANOPARTICLES IN MESOPOROUS SILICA FILMS

Various methods have been used for the production of stable Ag and Au nanoparticles in transparent mesoporous silicate matrices: 1) Production of Me/SiO_2 films from a silica precursor in the presence of metal salts at the sol–gel transition stage, their drying, and subsequent irradiation in the presence of a solution of benzophenone; 2) adsorption of gold (silver) ions on the surface of a previously synthesized porous film of SiO_2 followed by irradiation in the presence of a solution of benzophenone [86, 87].

Synthesis and Properties of Silica Films Doped with Silver Nanoparticles (Ag/SiO_2)

To produce films modified with silver the Ag^+ ions were inserted into a porous silica matrix by ion exchange with subsequent irradiation in an isopropyl alcohol solution of benzophenone (the Ag^+/SiO_2–BP solution system). The formation of the silver nanoparticles in the films is illustrated by the plasmon resonance spectra in Fig. 7a.

The figure shows the splitting of the resonance band into two modes. Two explanations can be given for such an effect: Splitting of the SPR bands may occur on account of the interaction of the closely located nanoparticles with each other [88] or on account of interaction in the transparent substrate [89], as which the SiO_2 film in this case behaves. The second suggestion

seems more reasonable if it is compared with the data obtained in solution, where the splitting of the SPR band in the absorption spectrum of the nanocolloid is not observed. With increase in the irradiation time of the Ag/SiO_2 film in a solution of benzophenone one of the maxima in the absorption spectrum of the reduced silver increases more quickly. The reason is possibly a decrease in the strength of the interaction with the surface during increase in the amount and size of the silver particles.

In order to prevent the silver nanoparticles from being washed out of the film into the solution and also to increase the amount of silver that can enter the film we used the method involving the introduction of $AgNO_3$ salt during preparation of the precursor for the sol–gel synthesis.

After heat treatment of the Ag^+/SiO_2 films with a silver content of 2% at 350 °C optically transparent films were obtained. During irradiation in an isopropyl alcohol solution of BP for 15 min with light of wavelength 365 nm the appearance of a yellow color was observed in the film, and in the spectrum there was a distinct absorption band with a maximum at 408 nm, which belongs to the SPR band of the silver nanoparticles.

To compare the effectiveness of the thermal and photochemical methods for the production of Ag nanoparticles in SiO_2 films the spectrum of the Ag/SiO_2 film after prolonged heat treatment (6 h) of Ag^+/SiO_2 at 500 °C is presented in Fig. 7c. The photogenerated Ag nanoparticles are smaller than the thermally generated ones on account of their tendency to aggregate at high temperatures.

From the scanning electron microscope (SEM) image of this film and calculation of the size distribution of the silver particles (Fig. 7b) it was found that their radius lies in the range of 2-7 nm. The distribution is bimodal in character, corresponding to the distribution of the pores in the film. The maximum size of the photogenerated Ag nanoparticles is obviously determined by the size of the pores in the silicate matrix. The obtained silver nanoparticles have a crystalline structure (Fig. 7d).

Synthesis and Properties of Films of Silica Doped with Gold Nanoparticles (Au/SiO_2)

In recent years the production of gold nanoparticles inserted into porous and nonporous inorganic matrices has been widely discussed in the literature [90-95]. Nanocomposite Au/SiO_2 films exhibit unusual optical characteristics due to interaction between the surface plasmon and applied electromagnetic field, e.g., high nonlinear optical sensitivity and surface-intensified Raman scattering [96], and can also find application as bactericidal coatings [95]. The Au/SiO_2 powders and films were usually produced by thermal decomposition of gold salts inserted into the silica matrix by impregnation or coprecipitation [91-93].

Mesoporous films of Au/SiO_2 were obtained by a photochemical method using a procedure similar to that used for the production of Ag/SiO_2 films and were compared with the films obtained by thermal decomposition of $HAuCl_4$ in the pores of SiO_2 [30].

Figure 8a shows the absorption spectra of silica films with molar ratio SiO_2 : Au = 0.01, produced by baking at various temperatures. The thermal transformations taking place with tetrachloroauric acid on heating are shown in the following scheme:

$$HAuCl_4 \xrightarrow{120\ ^\circ C} AuCl_3 \xrightarrow{185\text{–}200\ ^\circ C} AuCl \xrightarrow{290\ ^\circ C} Au.$$

As seen from Fig. 8a, after heating to 350 °C the fairly broad unsymmetrical SPR band of nanosized gold with a maximum at 553 nm is observed. At 350 °C not all the gold changes into the metallic state on account of thermally initiated autoreduction–autooxidation. At 450 °C all the gold ions are reduced, and during heat treatment at 500 °C only redistribution of the Au atoms occurs.

The SEM image presented in Fig. 8b proves the suggestion about the formation of both spherical and prismatic particles of gold. The corresponding size distribution of the gold nanoparticles indicates that during the thermal production of the Au/SiO_2 films at 500 °C very coarse particles of gold, the size of which significantly exceeds the pore size of the silica matrix, are formed. Apparently, at high temperatures the growth of the Au particles is not limited by the size of the pores, and the particle spreads out, and destroys the silica framework by growing into the SiO_2 walls.

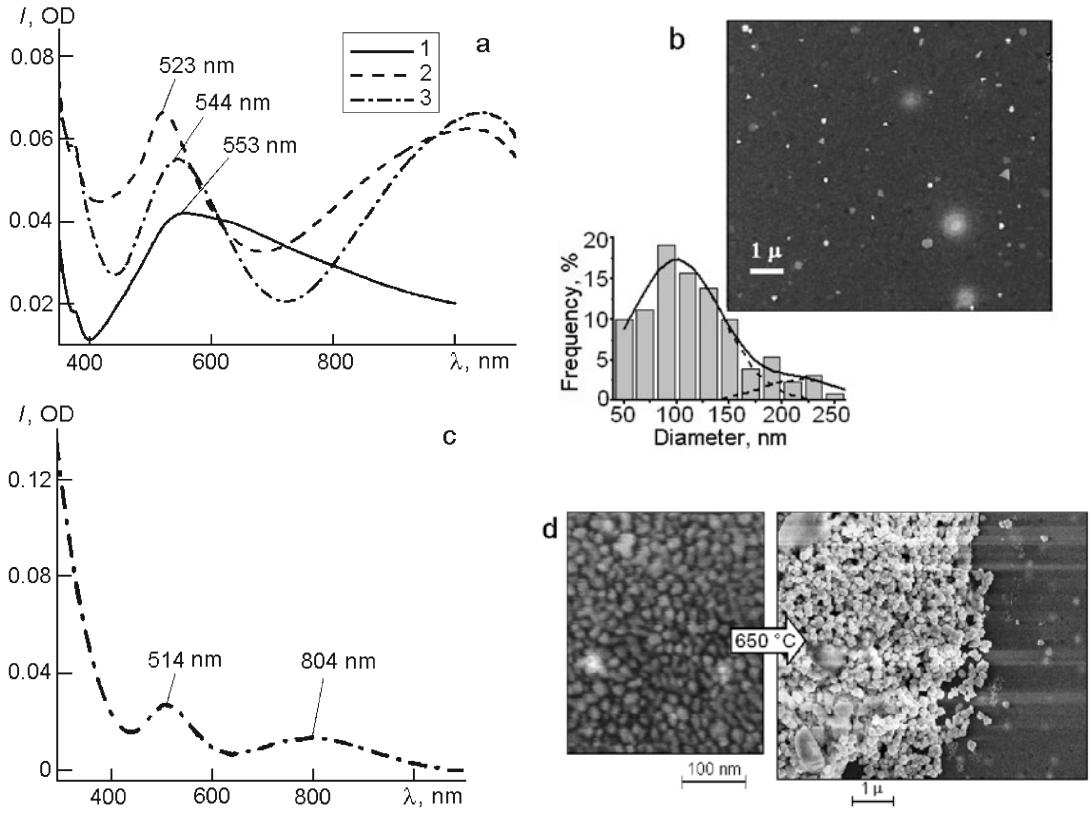

Fig. 8. a) The absorption spectra of the Au/SiO_2 films (1% Au) after baking for 3 h at 350 (1), 450 (2), and 500 °C (3). b) The SEM image of the Au/SiO_2 film (1% Au) after treatment for 3 h at 500 °C and the corresponding size distribution of the Au nanoparticles. c) The absorption spectra of a mesoporous SiO_2 film, into which the $AuCl_4^-$ ions were inserted by impregnation, after irradiation for 20 min (P123 was used as template agent during synthesis of the films). d) The SEM image of the Au/SiO_2 film (5% Au) obtained during UV irradiation and after baking at 650 °C.

For the purpose of the practical use of composite films of Au/SiO_2 both in optoelectronics and as antimicrobial coatings it is important to control the size and shape of the gold nanoparticles. In order to produce finer, spherical (with a diameter that would be set by the size of the pores), and monodisperse gold nanoparticles in a mesoporous silica matrix the method involving photochemical reduction of tetrachloroaurate ions in the pores of SiO_2 was used. After irradiation of the Au^{3+}/SiO_2 film for 20 min in an isopropyl alcohol solution of benzophenone distinct absorption bands with maxima at 514 and 804 nm appeared in the spectrum of the film (Fig. 8c).

The first band clearly corresponds to the plasmon absorption of the spherical gold particles, and the second to the longitudinal plasmon of particles of cylindrical form with a length-to-diameter ratio of ~4.1 [97]. Certain nanoparticles of gold clearly acquire cylindrical form in connection with the fact that their growth is restricted by the form and diameter of the pore in the silica films.

When the Au/SiO_2 films containing 5% Au are baked the gold nanoparticles diffuse to the surface of the film and gather, without coalescing, into aggregates (Fig. 8d). On the SEM picture the pores remaining after departure of the gold nanoparticles from the surface region of the film can be seen.

Thus, by impregnation followed by photosensitized reduction in an alcohol solution of benzophenone it is possible to obtain gold nanoparticles incorporated into the porous matrix of the silica film, and their size will not exceed the size of the pores.

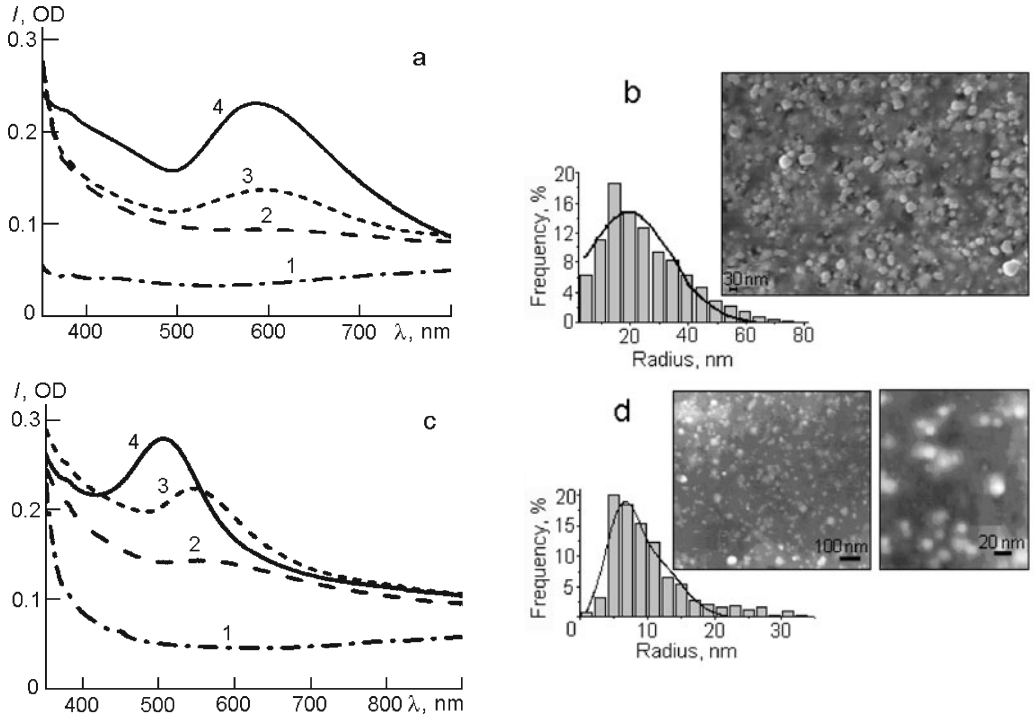

Fig. 9. a) The absorption spectra of the two-layer film: 1) Ag/SiO_2 layer; 2) Au/SiO_2 layer, 60 °C; 3) $Ag/SiO_2/Au/SiO_2$ after UV irradiation; 4) after treatment at 500 °C. b) The SEM image and size distribution of the nanoparticles of the $Ag/SiO_2/Au/SiO_2$ film after treatment at 500 °C. c) The absorption spectra of the two-layer film: 1) Au/SiO_2 layer, 60 °C; 2) Ag/SiO_2 layer; 3) $Au/SiO_2/Ag/SiO_2$ after UV irradiation; 4) after treatment at 500 °C. d) The SEM images and size distribution of the nanoparticles of the $Au/SiO_2/Ag/SiO_2$ film after treatment at 500 °C.

Synthesis and Properties of BMNP/SiO_2 Films

Mesoporous silica films containing bimetallic nanoparticles were prepared by the sol–gel method during the hydrolysis of tetraethoxysilane using the P123 triblock copolymer [$(PEO)_{20}$—$(PPO)_{70}$—$(PEO)_{20}$, molecular mass 5837] as template. The gold and silver ions were introduced by various methods: a) Both salts were dissolved simultaneously in the SiO_2 sol, and the hydrogel was then deposited on a glass substrate; b) films of the Ag^+/SiO_2 and Au^{3+}/SiO_2 hydrogels were deposited successively on the substrate, forming so-called "double-layer" films of silica – Ag/SiO_2 : Au/SiO_2 with clusters of gold or silver in the top layer. The films were subjected to UV irradiation by a 1000-W mercury lamp with incident light intensity $(1.4 \pm 0.1)\cdot 10^{17}$ quanta/s (for wavelength 254 nm) for 90 min followed by heat treatment at 500 °C.

As known, triblock copolymers are good reducing agents and stabilizers for the nanoparticles of noble metals [26].

The synthesis of the nanoparticles includes the following stages.

1) Adsorption of Ag^+ ($AuCl_4^-$) ions on the hydrophilic groups of the triblock copolymer:

$$Ag^+ + n\text{PEO—PPO—PEO} \rightarrow (Ag^+)\text{—(PEO—PPO—PEO)}_n,$$

2) Reduction of the metal ions by the action of UV irradiation:

$$(Ag^+)\text{—(PEO—PPO—PEO)}_n \xrightarrow{h\nu} Ag^0 + \text{oxidation products}$$

TABLE 1. The Stoichiometric Ratios of the Atoms in the Surface Layer of the Films (calculated from XPS data)

Element	Film $Au/SiO_2/Ag/SiO_2$	Film $Ag/SiO_2/Au/SiO_2$
Si	1.0	1.0
O	2.2	2.2
Au	0.005	0.013
Ag	0.006	0.023

where the oxidation products are carboxylate groups R_1COOR_2 ($R_{1,2}$ are organic groups) or $M(RCOO)_x$ (M is metal).
3) Adsorption of the atoms and formed clusters of nanoparticles on the surface of the hydrophobic PO groups:

$$Ag_m + l\text{PEO—PPO—PEO} \rightarrow Ag_m\text{—(PEO—PPO—PEO)}_l,$$

4) Growth of the metallic nanoparticles during heat treatment of the film.

The processes involved in the formation of the gold nanoparticles during irradiation occure in a complex of tetrachloroauric acid with the alcohol but differ somewhat from those for silver. After the appearance of the first portions of the gold nanoparticles catalytic (dark) reduction of the gold ions occurs. (If both ions are present in the solution the silver is also reduced on the surface of the gold nanoparticles.) In addition, during irradiation of the gold ions in the alcohol medium photogeneration of the nanoparticles also goes through by electron transfer inside the $AuCl_4^-$ from the chlorine ions to the gold ion. The mechanism of this photoreduction was described in [98]. It was established that 500 °C was sufficient for complete reduction of both ion salts in the silica matrix.

The idea of layer-by-layer deposition of Ag/SiO_2 and Au/SiO_2 hydrogels on one substrate with UV irradiation and heating of the precursors, proposed in [73], was used to level out the effect of the chloride ions, but we modified the procedure. The composition of the precursors remained the same as we usually employed in sol–gel syntheses of films [87]. Aluminum ions and a series of organic components that affect the formation of the nanoparticles of the metals were not added to the composition of the film in addition, and the procedure for the production of the bimetallic nanoparticles in SiO_2 was therefore significantly simplified in our experiment.

In particular, we investigated different sequences of deposition of the SiO_2 film with Ag(Au) ions on the substrate and their optical spectra and the morphology of the particles. For the film with a bottom layer of Ag/SiO_2 and a top layer of Au/SiO_2 after UV and heat treatment we observed the main absorption maximum at 587 nm, characteristic of the SPR of gold, and a shoulder at 400 nm corresponding to the SPR of the silver nanoparticles (Fig. 9a). In this case the metals probably form a composite with the Ag-core–Au-shell structure. Figure 9b shows the SEM images of these bimetallic nanoparticles on the surface and in the pores of the silica film, where the average radius is 20 nm. Nanoparticles on a scale of 30 nm with a lighter shell are visible, indicating the formation of the Ag-core–Au-shell structure. A similar conclusion from the spectrum of bimetallic nanoparticles was made in [99].

In the absorption spectrum of the two-layer film with a bottom layer of Au/SiO_2 the maximum of the SPR band is at 500 nm. The structure of the composite in this case is close to an alloy of the gold and silver nanoparticles. The position of the maximum of the SPR band does not correspond to that characteristic of the ratio Au : Ag = 1 : 1, i.e., 470-480 nm, and the

radius of the Ag-Au bimetallic nanoparticles, calculated from the microscope images, amounts to 5-10 nm (Fig. 9c, d). The top layer of the alloy is probably rich in silver nanoparticles, as confirmed by the data from X-ray photoelectron spectroscopy.

It is seen from the data in Table 1 that irrespective of the order of deposition of the layers of the precursor in the two-layer film the top layer is rich in silver nanoparticles. It must be remembered that the depth of penetration of the probing beam in the XPS method amounts to 7-10 nm, and the quantitative ratio of the atoms in the BMNP/SiO_2 composite relates specifically to this thin layer. During the formation of the core–shell structure the Au : Ag ratio in the top layer, determined from the data from XPS [87], amounts to 1 : 1.2. In the case of the alloy formed when the gold is situated in the bottom layer this ratio amounts to 1 : 1.8. It can be supposed that under the conditions of the synthesis the interface between the layers of the films disappears in the heat treatment process. The diffusion of the gold and silver nanoparticles and the formation of the structures of the bimetallic nanoparticles are realized in the general space of the uniform silica film at the stage of the sol–gel transition. Part of the silver nanoparticles in the bimetallic nanoparticles probably remains nonbonded, and they diffuse into the shell of the composite. Thus, the method of two-layer deposition of the hydrogel with the ions of the respective metals on the substrate makes it possible to obtain various types of Ag-Au bimetallic nanoparticles.

CATALYTIC ACTIVITY OF THE NANOPARTICLES

The catalytic activity of the nanosized particles was investigated in homogeneous (catalyst and reactant in the solution) and heterogeneous (catalyst attached to the support) media [4].

Bulk gold does not have catalytic activity. Small clusters of gold exhibit high catalytic activity on the surface of titanium dioxide in the processes of selective oxidation of CO in hydrogen [100, 101]. The Ag/SiO_2 composite was also investigated successfully in the same process [102]. In the opinion of the authors the reactivity depends on the electronic and chemical characteristics of the nanoparticles and also on their shape, size, and degree of oxidation. The nature of the substrate is also responsible for catalytic activity [103]. The Ag-SiO_2-Al_2O_3 composites are also highly active catalysts for the formation of formaldehyde in the partial oxidation of methanol [104].

Titanium and silicon oxides doped with gold and silver nanoparticles also exhibit high photocatalytic activity.

The degradation of organic substances (dyes, antibiotics, etc.) takes place by a mechanism of so-called plasmon photocatalysis (PC). Plasmon photocatalysis involves increasing the amplitude of the electric field on the surface of the noble metal nanoparticle by UV irradiation. The idea of plasmon photocatalysis was put forward in [2] for the case of Ag/TiO_2. The absorption bands of anatase and the SPR of silver are closely located, and during irradiation there is a substantial increase in the near electric field in the vicinity of the silver nanoparticle. The authors supposed that this increased field stimulates excitation of an electron–hole pair in the TiO_2 and thereby increases the effectiveness of the photocatalytic action. The plasmon-induced transfer of an electron from a gold nanoparticle measuring 10 nm to TiO_2 nanoparticles was detected by means of the instant absorption spectra during femtosecond laser excitation for 240 fs. Since the nanoparticles of gold have a very high absorption coefficient compared with the usual dye molecules they can be used as effective sources of electrons in nanodevices in the case where the reverse transfer of an electron is suppressed [105]. In a composite with the dielectric SiO_2 the excited electrons on the surface of the nanoparticle of the noble metal during interaction with molecular oxygen form a superoxide radical, from which a hydroxo radical that decomposes organic molecules is formed. In order to compare the photocatalytic activity of Me/TiO_2 and Me/SiO_2 composites, where Me is Ag or Au, the rate constants of decomposition of the antibiotic tetracycline hydrochloride (TC) were determined. Tetracycline is a real contaminant of effluents and moreover has an absorption band in the visible region of the spectrum, and its decomposition is conveniently monitored from the change in the absorption spectrum. Tetracycline was therefore chosen as model toxic substance. In the presence of a film of Au/SiO_2 the rate constant for the degradation of tetracycline is equal to $5.7 \cdot 10^5$ s^{-1}, and for Ag/SiO_2 it is $5.0 \cdot 10^5$ s^{-1} [106]. Between ln (C_0/C) and the reaction time there is a linear dependance, indicating that the process occurs by a first-order kinetic mechanism. When films based on titanium dioxide with nanoparticles of the metals are used the rate is higher than with Me/SiO_2. However, the advantages of a catalyst based on silica compared with that based on titanium dioxide are the substantially higher thermal stability and the possibility of regeneration [107].

BACTERICIDAL CHARACTERISTICS OF STABILIZED SILVER NANOSTRUCTURES ON THE SURFACE OF DISPERSED SILICA

On account of their highly developed surface the nanoparticles of metals have high reactivity in chemical and biological processes. The nanoparticles of Ag and Au are used for the delivery of drugs [108-110], the treatment of wounds, the decontamination of water, and as bactericidal agents [111-115]. On account of the strong electric fields on the surface of gold nanoparticles the absorption and scattering of electromagnetic radiation are significantly stronger. These unique characteristics enable the creation of new reagents for molecular imaging and for the photothermal therapy of oncological diseases [5, 116, 117]. Many bacteria are resistant to antibiotics, and it is therefore necessary to look for new bactericidal materials. Silver nanoparticles have a broad spectrum of antibacterial activity and are nontoxic for humans at low concentrations. The toxicity of the nanoparticles is discussed in [118]. In large amounts, however, their toxicity is high, and the biocompatibility is substantially lower than for gold nanoparticles [119-122].

We showed that the biocidal characteristics of gold nanoparticles show up well when they are used at the growth stage of *E. coli*, while silver nanoparticles are effective during the elimination of already grown colonies [123-125]. The effectiveness of the nanoparticles can be intensified by depositing them on a support with a highly developed surface. In this respect highly dispersed silica (HDS) is an ideal material. An important problem in the synthesis of nanoparticles is prevention or retardation of their aggregation and also oxidation at the stage of formation of the silver nanoclusters.

Stabilization of Silver Nanoparticles on the Surface of Dispersed Silica

In order to protect the silver nanoparticles from oxidation and aggregation their synthesis is conducted in restricted spaces: Inverse micelles, porous matrices, polymers, oxide films, etc. [126, 127]. As mentioned, the silver nanoparticles inserted into the silica film retain their bright-yellow color and characteristic SPR band in the absorption spectrum for many months. They are protected from contact with the surroundings by the surface of the SiO_2 film. During prolonged storage of a colloidal solution of silver nanoparticles in contact with air oxidation processes occur with the formation of a thin oxide layer around the nanoparticles, leading to a decrease in the intensity and a small shift of the SPR band [128]. The layer of stabilizer around the nanoparticles protects them from complete oxidation in the solution.

Conversely, on the surface of the dispersed silica during direct contact with air rapid oxidation of the silver nanoparticles occurs with the formation of the oxide: $4Ag^0 + O_2 \leftrightarrow 2Ag_2O$. This shows up in the bleaching of the sample and the disappearance of the SPR band in the absorption spectra at 400 nm over a short period of time (10-15 min). The silver oxide formed here decomposes on repeated heating to 250-300 °C with restoration of the characteristic yellow color, which disappears again when the Ag/SiO_2 powder cools to room temperature.

Thus, in contrast to their state in the films, on the surface of dispersed silica the silver nanoparticles are unstable. Therefore, in view of the diversity of potential applications of dispersed silica containing Ag nanoparticles on the surface, particularly as bactericidal agents, the stabilization of the nanoparticles of silver and their protection against oxidation and the influence of the surroundings represent an urgent task from the theoretical and applied view point. Various methods have been used for the treatment of the catalysts: Treatment of $AgNO_3/SiO_2$ in a stream of hydrogen followed by heating in an atmosphere of oxygen results in oxidation of silver with subsequent decomposition of the oxide layer and penetration of oxygen inside the silver nanoparticles [102]; the authors of [100] proposed to remove the OH groups from the surface of the silica and thereby increase the stability and degree of dispersion of the Ag; the authors of [129] propose calcination a mechanical mixture of silver with silica at 500 °C. In [52] it was suggested that a strong covalent bond is formed between the Ag and defect centers in the SiO_2. By means of the X-ray photoelectron spectra the authors of [130] were able to confirm the oxidation of silver nanoparticles during heat treatment. More recently [131] the thermal stability of the nanoparticles after low-temperature plasma treatment of Ag in O_2 and then in H_2 was demonstrated. However, most papers have been directed toward the formation of a protective shell around the nanoparticles during their deposition.

Stabilization of the Ag nanoparticles in solutions is realized with the use of surfactants (SFA) or polymers – PEO, PVP, etc. [22, 23]. Thus, the surfactant sodium oleate is adsorbed on the surface of the silver nanoparticles with the formation of a

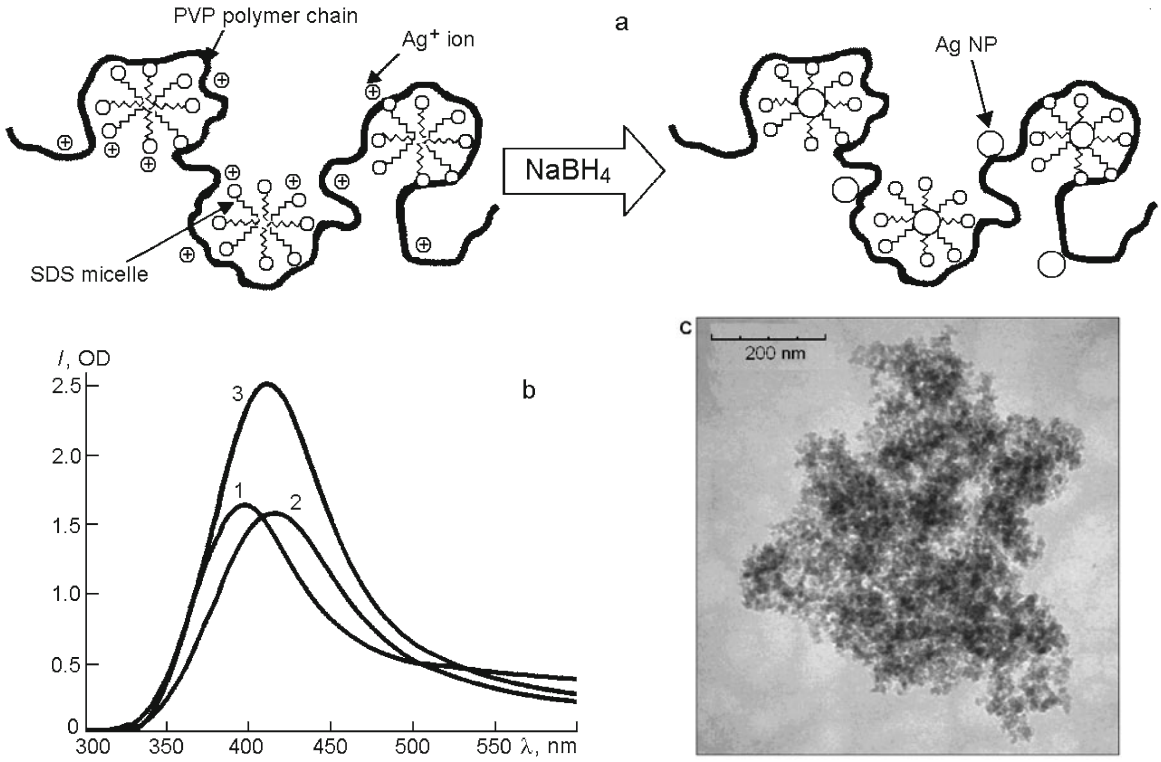

Fig. 10. a) Diagram of the interaction between the complex of PVP with SDS and the silver ions and nanoparticles after reduction with tetrahydroborate. b) Diffuse reflection spectra of powders of silica with silver nanoparticles stabilized with SDS (1), SDS/PVP (2), and PVP (3). c) TEM of Ag/SiO_2 powder (0.05% Ag).

protective layer [24]. The Ag nanoparticles obtained during the high-temperature solvolysis of an ethanol solution of $AgNO_3$ in the presence of dodecanethiol also remain stable after drying [25]. The principle of the stabilization of Ag nanoparticles with polymers or surfactants was applied successfully to the synthesis of composite systems based on highly dispersed silica (HDS) containing stable nanoparticles of silver with PVP and/or SDS as stabilizers [124, 125].

Samples of Ag/SiO_2 were synthesized by the adsorption of previously prepared colloidal solutions of nanosized silver on the surface of dispersed silica.

Nanosized silver in colloidal solution was obtained by chemical reduction from silver nitrate in the presence of sodium tetrahydroborate and a binary stabilizer – SDS and PVP. The obtained silver colloids were adsorbed on the surface of HDS. The concentration of Ag on the HDS amounted to 0.05%.

The use of a binary stabilizer raises the stability of the silver nanoparticles. The interaction of the SDS and PVP consists of a combination of two processes: the formation of a complex as a result of hydrophobic interaction between the hydrocarbon unit of the SDS and the methylene groups of the PVP and electrostatic interaction between the head groups of the SDS and the partial charges of the nitrogen and oxygen of the pyrrolidol ring [132-134]. A section of the polymer partly penetrates and envelops the micelle of the surfactant (Fig. 10a).

Optical Characteristics of Silver Nanoparticles on the Surface of Highly Dispersed Silica

The binding of silver clusters by the surface of HDS takes place actively as a result of interaction of the molecules of stabilizers containing solubilized Ag nanoparticles with the functional OH groups of the silica. The Ag/SiO_2 powders retain their intense bright color for a long time.

TABLE 2. Antimicrobial Properties of Colloidal Solutions of Silver Nanoparticles, log *R*

Sample (concentration)	Exposure, h	Test strains		
		E.coli	*S.aureus*	*C.albicans*
Ag NP (0.0016%)	1	>5.22	<1.57	>4.27
	2	>5.22	2.07	>4.27
	4	>5.22	4.35	>4.27
	24	>5.22	>5.24	>4.27
Ag NP (0.0008%)	1	4.07	<1.57	>4.27
	2	5.11	<1.57	>4.27
	4	>5.22	2.72	>4.27
	24	>5.22	>5.24	>4.27
Ag NP (0.0004%)	1	3.97	<1.57	>4.27
	2	5.07	<1.57	>4.27
	4	>5.22	<1.57	>4.27
	24	>5.22	5.09	>4.27
Initial amount of microorganisms, log*		7.37	7.39	6.42

The high adsorption capacity of HDS toward nanoparticles coated by stabilizers should be noted. Up to a content of 0.05 wt.% silver nanoparticles are not washed off and are not extracted from the surface of the HDS. Figure 10b shows the diffuse reflection spectra of HDS powders containing 0.05 wt.% of silver calculated by the Kubelka–Munk equation with various stabilizers of nanoparticles. The position of the SPR band is closely located for all the composites. The intensity of the bands changes very little with time. It is interesting to note that in the presence of PVP the intensity of the SPR band is noticeably higher compared with SDS or a mixture of SDS and PVP. This can be explained both by the higher degree of dispersion of the nanoparticles in the presence of PVP [135] and by coagulation of the HDS in the aqueous solution in the presence of SDS. According to [136] the interaction of the colloidal particles of silica in water in the presence of SDS when they have formed a sufficient amount of micelles changes from repulsion to mutual strong attraction. In [137] it was shown that after drying at room temperature such silica composites form three-dimensional porous structures.

The silica particles are solubilized inside the micelles containing silver nanoparticles. It can be supposed that in the drying process the nanoparticles of silver situated in the SDS micelles are encapsulated by the silica, and as a consequence of this their contribution to the SPR band is reduced.

The position of the maxima of the SPR bands of the silver nanoparticles in the colloidal solution and in the adsorbed state practically coincides. The shell of stabilizer around the Ag nanoparticles on the surface of the SiO_2 is stable up to temperatures of 85-90 °C [124, 125].

The electron-microscope image of Ag/SiO_2 (Fig. 10c) shows uniform coverage of the spherical particles of HDS (light circles) by silver particles (dark circles).

TABLE 3. Antimicrobial Properties of Suspensions of Silver Nanoparticles on Silica Surface, log *R*

Sample (concentration)	Exposure, h	Test strains		
		E.coli	*S.aureus*	*C.albicans*
Ag NP (0.0016%)/	1	<1.39	3.89	>4.54
SiO_2 (3.13%)	2	1.48	5.14	>4.54
	4	3.58	>5.17	>4.54
	24	>5.06	>5.17	>4.54
SiO_2 (3.13%)	1	<1.39	<1.5	<0.87
(control)	2	<1.39	<1.5	<0.87
	4	<1.39	<1.5	<0.87
	24	<1.39	<1.5	<0.87
Initial amount of microorganisms, log*		7.21	7.32	6.69

Antimicrobial Properties of Suspensions of Ag/SiO_2 Nanoparticles

The antimicrobial properties were studied by the suspension method according to the European standards [138, 139]. The antimicrobial activity of the Ag/SiO_2 systems against *Staphylococcus aureus* ATC C 6538, *Escherichia coli* K12 NCTC 10538, and *Candida albicans* ATCC 10231 was determined.

Many publications have been devoted to investigation of the antimicrobial potential of nanosized silver ([140, 141] and references therein). The bactericidal characteristics of composite materials based on films and granules of silica gel with silver nanoparticles have also been discussed in the literature. Thus, in [142] the authors obtained bactericidal material containing clusters of silver on microspheres of silica gel doped with aluminum ions. Colorless materials, from which however the silver ions were washed out by water at 37 °C (according to the authors), were obtained. In this case, evidently, silver nanoparticles are not formed in the oxide matrix, and the bactericidal activity is provided by the silver ions. In [143] the bactericidal properties of spherical silica gel covered with islands of silver against *E. coli* and *S. aureus* were studied. At the maximum content of Ag/SiO_2 of 1 mg/mL the population of both microbes is reduced by 72%. The procedures for the production of the samples are not presented in this paper.

We obtained stable colloidal solutions of nanosized silver with very low concentrations of nanoparticles – 0.0016, 0.0008, 0.0004% Ag – in the presence of SDS and PVP and also suspensions of HDS with silver nanoparticles (Ag/SiO_2 nanoparticles with concentrations Ag 0.0016%, HDS 3.13%) using the SDS/PVP complex as stabilizer and determined their antimicrobial activity with respect to three cultures – *E. coli*, *S. aureus*, and *C. albicans* (Table 2). The required reduction for the bacteria (5 log) and fungi (4 log) began after 1 h contact of the nanosilver with the microbe cells. The resistance of the staphylococci to the nanosilver was significantly higher (reduction 4.35 log after 4 h exposure).

A solution of $AgNO_3$ with the same concentration as in the solution of colloidal particles did not have any microbiocidal activity. Sodium dodecyl sulfate and polyvinylpyrrolidone did not have antimicrobial activity.

The obtained results from investigation of the antimicrobial activity of a suspension of HDS containing silver nanoparticles (Ag/SiO_2 NP) are presented in Table 2. The insertion of Ag nanoparticles into a suspension of SiO_2 somewhat reduced the activity of the silver, which resulted in an increase of the exposure time and a change in the nature of the interaction of the Ag nanoparticles with the bacterial cell.

The antimicrobial activity of the Ag NPs/SiO_2 complex remained high: after contact the required reduction was observed after 2 h in *S. aureus* and even earlier in *C. albicans*, while the required effect with *E. coli* began after 4 h exposure.

The data that we obtained, presented in Table 3, indicate practically complete suppression of the growth of all the investigated bacteria with extremely small concentrations of nanosized silver. In comparison with the data presented in the literature the required concentrations were 10-100 times lower.

The prospects for the use of composites containing the nanoparticles of noble metals seem limitless: the creation of a new class of drugs and diagnostic systems; fluorescence enhancement of molecular markers in biosystems; enhancement of the Raman and Rayleigh scattering in nonlinear optical devices; the production of a new class of bactericidal materials and coatings; etc.

REFERENCES

1. M. A. El-Sayed, *Account. Chem. Res.*, **34**, No. 4, 257 (2001).
2. K. Awazu, M. Fujimaki, C. Rockstuhl, et al., *J. Am. Chem. Soc.*, **130**, 1676 (2008).
3. P. K. Jain, X. Huang, I. H. El-Sayed, and M. A. El-Sayed, *Plasmonics*, **2**, No. 3, 107-118 (2007).
4. R. Narayanan and M. A. El-Sayed, *J. Phys. Chem. B*, **109**, No. 26, 12663 (2005).
5. X. Huang, P. K. Jain, I. H. El-Sayed, and M. A. El-Sayed, *Nanomedicine*, **2**, No. 5, 681 (2007).
6. P. V. Kamat, *J. Phys. Chem. B*, **106**, 7729 (2002).
7. L. Liz-Marzan, *Mater. Today*, **7**, 26 (2004).
8. L. Bois, F. Bessueille, E. Chassagneux, et al., *Colloids Surfaces A*, **325**, No. 1/2, 86 (2008).
9. M. P. Pileni, I. Lisiecki, L. Motte, et al., *Progr. Colloid Polym. Sci.*, **93**, 1 (1993).
10. N. Toshima, T. Yonezava, and K. Kushihashi, *J. Chem. Soc., Faraday Trans.*, **89**, 2537 (1993).
11. Z. Zang, H. Cheng, and J. Ma, *J. Mater. Sci. Lett.*, **20**, 439 (2001).
12. S. Shibata, K. Aoki, T. Yano, and M. Yamane, *J. Sol-Gel Sci. Technol.*, **11**, 279 (1998).
13. S. Lambert, C. Cellier, P. Grande, et al., *J. Catal.*, **221**, 335 (2004).
14. H. Bi, W. Cai, H. Shi, and X. Liu, *Chem. Phys. Lett.*, **357**, 249 (2002).
15. W. Chen, W. Cai, C. Liang, and L. Zhang, *Mater. Res. Bull.*, **136**, 335 (2001).
16. V. Pol, D. Srivatsava, O. Palchik, et al., *Langmuir*, **18**, 3352 (2002).
17. S. Tang, S. Zhu, H. Lu, and X. Meng, *J. Solid State Chem.*, **181**, 587 (2008).
18. R. A. Caruso, M. Ashokkumar, and F. Grieser, *Langmuir*, **18**, No. 21, 7831 (2002).
19. C.-H. Su, P.-L. Wu, and C.-S. Yeh, *J. Phys. Chem. B.*, **107**, No. 51, 14240 (2003).
20. K. Okitsu, M. Ashokkumar, and F. Grieser, *J. Phys. Chem. B.*, **109**, No. 44, 20673 (2005).
21. S. Huang, H. Ma, X. Zhang, et al., *J. Phys. Chem. B.*, **109**, No. 42, 19823 (2005).
22. J. P. Wilcoxon, R. L. Williamson, and R. Baughman, *J. Chem. Phys.*, **98**, 9933 (1993).
23. Y. N. Cheomg Chan, R. R. Schrock, and R. E. Cohen, *Chem. Mater.*, **4**, 24 (1992).
24. W. Wang, S. Efrima, and O. Regev, *Langmuir*, **14**, 602 (1998).
25. Ch. Tian, B. Mao, E. Wang, et al., *Nanotechnology*, **18**, 285607 (2007).
26. T. Sakai and P. Alexandridis, *J. Phys. Chem. B*, **109**, No. 16, 7766 (2005).
27. T. Sato, N. Maeda, H. Ohkoshi, and Y. Yonezawa, *Bull. Chem. Soc. Jap.*, **67**, 3165 (1994).
28. G. V. Krylova, A. M. Eremenko, N. P. Smirnova, and S. Eustis, *Teor. Éksp. Khim.*, **41**, No. 2, 100-104 (2005). [*Theor. Exp. Chem.*, **41**, No. 2, 105-110 (2005) (Engl. Transl.).]
29. G. Krylova, A. Eremenko, N. Smirnova, and S. Eustis, *Int. J. Photoenergy*, **7**, 193 (2005).
30. G. V. Krylova, A. M. Eremenko, N. P. Smirnova, and S. Eustis, *Teor. Éksp. Khim.*, **41**, No. 6, 348-353 (2005). [*Theor. Exp. Chem.*, **41**, No. 6, 365-370 (2005) (Engl. Transl.).]

31. S. Eustis, G. Krylova, A. Eremenko, et al., *J. Photochem. Photobiol. A*, **181**, 385 (2006).
32. N. J. Turro, M. B. Zimmt, and I. R. Gould, *J. Am. Chem. Soc.*, **107**, 5826 (1985).
33. W. Cheng and E. Wang, *J. Phys. Chem. B*, **108**, 24 (2004).
34. A. Henglein, *Chem. Mater*., **10**, 444 (1998).
35. A. Henglein, *Langmuir*, **15**, 6738 (1999).
36. V. C. Daniel and D. Astruk, *Chem. Rev.*, **104**, 293 (2004).
37. S. Eustis, H.-Y. Hsu, and M. A. El-Sayed, *J. Phys. Chem. B*, **109**, 4811 (2005).
38. C. D. Wagner, W. M. Riggs, L. E. Davis, et al., *Handbook of X-Ray Photoelectron Spectroscopy*, Perkin-Elmer Corp., Eden Prairie, Minn. (1979), p. 55344.
39. R. Averitt, S. Westcott, and N. Halas, *J. Opt. Soc. Am.*, **16**, 1824 (1999).
40. Y. Lu, Y. Yin, Z. Li, and Y. Xia, *Nano Lett.*, **2**, 785 (2002).
41. Y. Kim, D. Lee, H. Cha, et al., *J. Phys. Chem. C*, **111**, 3629 (2007).
42. Q. Sun, Q. Wang, B. K. Rao, and P. Jena, *Phys. Rev. Lett.*, **93**, No. 18, 29 (2004).
43. N. Lopez, F. Illas, and G. Pacchioni, *J. Phys. Chem. B*, **103**, 1712 (1999).
44. N. Lopez, F. Illas, and G. Pacchioni, *J. Am. Chem. Soc.*, **121**, 813 (1999).
45. G. Pacchioni, N. Lopez, and F. Illas, *Faraday Discuss.*, **209**, 222 (1999).
46. Y. D. Kim, J. Stultz, T. Wei, and D. W. Goodman, *J. Phys. Chem. B*, **106**, 6827 (2002).
47. G. Haas, A. Menck, H. Brune, et al., *Phys. Rev. B*, **61**, 11105 (2000).
48. M. Baumer, M. Frank, M. Heemeier, et al., *J. Surface Sci.*, **454**, 957 (2000).
49. B. K. Min, W. T. Wallace, A. K. Santra, and D. W. Goodman, *J. Phys. Chem. B.*, **108**, 16339 (2004).
50. U. Heiz and W. D. Schneider, *J. Phys. D*, **33**, R85 (2000).
51. S. Abbet, A. Sanchez, U. Heiz, et al., *J. Am. Chem. Soc.*, **122**, 3453 (2000).
52. Y. D. Kim, T. Wei, S. Wendt, and D. W. Goodman, *Langmuir*, **19**, 7929 (2003).
53. M. Komiyama and T. Shimaguchi, *Surface Interface Anal*., **32**, 189 (2001).
54. S. Hua-Zhong, Y. Bao-Dian, Z. Li-De, et al., *Chin. Phys. Lett.*, **17**, 537 (2000).
55. X. Hu, Q. Zhao, X. Jiang, et al., *Solid State Commun.*, **138**, 43 (2006).
56. E. Snoeks, A. van Blaaderen, T. van Dillen, et al., *Adv. Mater.*, **12**, 1511 (2000).
57. C. Graf, D. Vossen, A. Imhof, and A. van Blaaderen, *Langmuir*, **19**, 6693 (2003).
58. W. Cai, H. Hofmeister, and T. Rainer, *Physica E*, **11**, 339-344 (2001).
59. F. X. Shi, L. L. Cao, W. Q. Yao, and X. Y. Ye, *J. Mater. Sci.*, **35**, Nos. 14/15, 3655-3658 (2000).
60. S. Kundu, M. Mandal, S. K. Ghosh, and T. Pal, *J. Colloid Interface Sci.*, **272**, 134 (2004).
61. T. Siebrands, M. Giersig, P. Mulvaney, and Ch.-H. Fischer, *Langmuir*, **9**, 2297 (1993).
62. S. Link, Z. L. Wang, and M. A. El-Sayed, *J. Phys. Chem. B*, **103**, 3529 (1999).
63. S. Devarajan, B. Vimalan, and S. Sampath, *J. Colloid Interface Sci.*, **278**, 126 (2004).
64. J. H. Hodak, A. Henglein, and G. V. Hartland, *J. Phys. Chem.*, **104**, 9954 (2000).
65. L. Qian and X. Yang, *Colloids Surfaces A*, **260**, 79 (2005).
66. I. Srnová-Šloufová, F. Lednický, A. Gemperle, and J. Gemperlová, *Langmuir*, **16**, 9928 (2000).
67. P. Mulvaney, *Langmuir*, **12**, 788 (1996).
68. Liu Yu-Chuan, Yu Chung-Chin, and Hsu Ting-Chu, *Electrochem. Commun.*, **9**, 639 (2007).
69. R. Xiangling, M. Xianwei, and T. Fangqiong, *Sensors Actuators B*, **110**, 358 (2005).
70. C. A. Morris, M. L. Anderson, R. M. Stroud, et al., *Science*, **284**, 622 (1999).
71. H. Kozuka and S. Sakka, *Chem. Mater.*, **5**, 222 (1993).
72. F. Akbarian, B. Dunn, and J. Zink, *J. Phys. Chem.*, **99**, 3892 (1995).
73. S. Pal and G. De, *Chem. Mater.*, **17**, 6161 (2005).
74. L. Longenberger and G. Mills, *J. Phys. Chem.*, **99**, 475 (1995).
75. M. Mandal, S. Kundu, S. K. Ghosh, and T. Pal, *J. Photochem. Photobiol. A*, **167**, 17 (2004).
76. G. Mattei, C. Maurizio, C. Sada, et al., *J. Non-Crystal. Solids.*, **345/346**, 667 (2004).
77. S. Eustis, G. Krylova, A. Eremenko, et al., *Photochem. Photobiol. Sci.*, **4**, No. 1, 154 (2005).
78. G. Schmid, *Chem. Rev.*, **92**, 1709 (1992).

79. C. H. Rochester and D.-A. Trebilco, *J. Chem. Soc., Faraday Trans. I*, **75**, 2211 (1978).
80. G. Krylova, A. Eremenko, N. Smirnova, and A. Korchev, *Chemistry, Physics, and Technology of Surfaces*, **10**, 60 (2004).
81. N. Smirnova, A. Eremenko, I. Petrik, et al., *J. Sol-Gel Sci. Technol.*, **32**, 357 (2004).
82. C. G. Hatchard and C. A. Parker, *Proc. Roy. Soc. London A*, **235**, 518 (1956).
83. A. Henglein, *J. Phys. Chem.*, **97**, 5457 (1993).
84. E. Gachard, H. Remita, J. Khatouri, et al, *New J. Chem.*, 1257 (1998).
85. G. Porter and F. Wilkinson, *Trans. Faraday Soc.*, **57**, 1686 (1961).
86. H. Yashan, A. Eremenko, N. Smirnova, et al., *NATO Sci. Peace Security Ser. C*, P. Innocenzi, Yu. Zub, V. Kessler (eds.), 473 (2008).
87. A. M. Eremenko, G. R. Yashan, G. V. Krylova, et al., *Teor. Éksp. Khim.*, **44**, No. 6, 348-353 (2008). [*Theor. Exp. Chem.*, **44**, No. 6, 356-361 (2008) (Engl. Transl.).]
88. Yu-lin Xu., *Appl. Opt.*, **34**, 4573 (1995).
89. C. Beitia, Y. Borensztein, R. Lazzari, et al., *Phys. Rev. B*, **60**, 6018 (1999).
90. P. Mukherjee, Ch. R. Patra, R. Kumar, and M. Sastry, *Phys. Chem. Commun.*, **5**, 1 (2001).
91. S. T. Selvan, Y. Ono, and M. Nogami, *Mater. Lett.*, **37**, 156 (1998).
92. S. Bharathi, N. Fishelson, and O. Lev, *Langmuir*, **15**, No. 6, 1929 (1999).
93. J. Matsuoka, R. Naruse, H. Nasu, and K. Kamiya, *J. Non-Crystal. Solids*, **218**, 151 (1997).
94. M. Epifani, C. Giannini, L. Tapfer, and L. Vasanelli, *J. Am. Ceram. Soc.*, **88**, 2385 (2000).
95. M. Mennig, M. Schmitt, U. Becker, et al., *Proc. SPIE, Sol-Gel Opt. III*, **2288**, 130 (1994).
96. J. Matsuoka, R. Mizutani, S. Kaneko, et al., *J. Ceram. Soc. Jpn.*, **101**, 53 (1993).
97. S. Link and M. A. El-Sayed, *J. Chem. Phys.*, **114**, 2362 (2001).
98. S. Eustis, H.-Y. Hsu, and M. A. El-Sayed, *J. Phys. Chem. B,* **109**, 4811 (2005).
99. S. Shiv Shankar, A. Rai, A. Ahmad, and S. Murali, *J. Colloid Interface Sci.*, **275**, 496 (2004).
100. Z. Qu, W. Huang, S. Zhou, et al., *J. Catal.*, **234**, 33 (2005).
101. M. Valden, X. Lai, and D. W. Goodman, *Science*, **281**, 1647 (1998).
102. Z. Qu, M. Cheng, C. Shi, and X. Bao, *J. Natural Gas Chem.*, **14**, 4 (2005).
103. M. S. Chen and D. W. Goodman, *Science*, **306**, 252 (2004).
104. W.-L. Dai, Y. Cao, L.-P. Ren, et al., *J. Catal.*, **228**, 80 (2004).
105. A. Furube, L. Du, K. Hara, et al., *J. Am. Chem. Soc.*, **129**, 14852 (2007).
106. G. R. Yashan, O. P. Linnik, G. M. Eremenko, and N. P. Smirnova, *Khim., Fiz. Tekhnol. Poverkhn.*, **15**, 246 (2009).
107. G. Veith, A. Lupini, S. Rashkeev, et al., *J. Catal.*, **262**, No. 1, 92 (2009).
108. J. L. West and N. J. Halas, *Ann. Rev. Biomed. Eng.*, **5**, 285 (2003).
109. G. F. Paciotti, L. Myer, D. Weinreich, et al., *Drug Delivery*, **11**, 169 (2004).
110. K. K. Jain, *Technol. Cancer Res. Treat.*, **4**, 407 (2005).
111. J. L. Elchiguuerra, J. L. Burt, J. R. Morones, et al., *J. Nanobiotechnol.*, **3**, 1477 (2005).
112. C. Baker, A. Pradhan, L. Pakstis, et al., *J. Nanosci. Nanotechnol.*, **5**, 244 (2005).
113. S. Shrivastava, T. Bera, A. Roy, et al., *Nanotechnology*, **18**, 1 (2007).
114. S. Pal, Y. Tak, and J. M. Song, *Appl. Environ. Microbiol.*, **73**, 1712 (2007).
115. E. Weir, A. Lawlor, A. Whelan, and F. Regan, *Analyst*, **33**, 835 (2008).
116. P. K. Jain, K. S. Lee, I. H. El-Sayed, and M. A. El-Sayed, *J. Phys. Chem. B*, **110**, No. 14, 7238 (2006).
117. X. Huang, I. H. El-Sayed, W. Qian, and M. A. El-Sayed, *J. Am. Chem. Soc.*, **128**, 2115 (2006).
118. Y. Jin and X. Zhao, *Cytotoxicity of Photoactive Nanoparticles, Safety of Nanoparticles. Ser. Nanostructure Science and Technology*, Springer, New York (2009).
119. P. Nallathamby, K. Lee, and X. Xu, *ACS Nano*, **2**, 1371 (2008).
120. L. Browning, K. Lee, T. Huang, et al., *Nanoscale*, **1**, 138 (2009).
121. Y. Song, P. Nallathamby, T. Huang, et al., *J. Phys. Chem. C.*, **114**, No. 1, 74 (2010).
122. T. Huang, P. Nallathamby, and X. Xu, *J. Am. Chem. Soc.*, **130**, 17095 (2008).
123. G. R. Yashan, G. V. Krylova, A. M. Eremenko, et al., *Khim., Fiz. Tekhnol. Poverkhn.*, **14**, 524 (2008).

124. Yu. Mukha, A. M. Eremenko, N. P. Smirnova, et al., *Khim., Fiz. Tekhnol. Poverkhn.*, **15**, 255 (2009).
125. I. Mukha, A. Eremenko, G. Korchak, and A. Mikhienkova, *J. Water Resource Protection*, **2**, 131 (2010).
126. E. D. Goddard and J. V. Gruber (eds.), *Principles of Polymer Science and Technology in Cosmetics and Personal Care*, Marcel Dekker, New York (1999).
127. R. Patakfalvi, Z. Viranyi, and I. Dekany, *Colloid Polym. Sci.*, **283**, 299 (2004).
128. L. G. Grechko, A. M. Eremenko, G. V. Krylova, et al., *Visn. Kyiv. Un-tu., Ser. Fiz.-Mat. Nauky*, **4**, 450 (2004).
129. J. Qu, H. Li, H. Liu, and H. He, *Catal. Today*, **90**, 291 (2004).
130. W. Li, S. Seal, E. Megan, et al., *J. Appl. Phys.*, **93**, No. 12, 9553 (2003).
131. K. Yliniemi, P. Ebbinghaus, P. Keil, et al., *Surface Coat. Technol.*, **201**, 7865 (2007).
132. M. Prasad, R. Palepu, and S. P. Moulik, *Colloid Polym. Sci.*, **284**, No. 8, 871-878 (2006).
133. G. Olofsson and G. Wang, *Pure Appl. Chem.*, **66**, No. 3, 527-532 (1994).
134. P. Roscigno, F. Asaro, G. Pellizer, et al., *Langmuir*, **19**, 9638-9644 (2003).
135. S. Papp, R. Patakfalvi, and I. Dekany, *Croat. Chem. Acta*, **80**, Nos. 3/4, 493 (2007).
136. S. R. Kline and E. W. Kaler, *Langmuir*, **12**, No. 10, 2402 (1996).
137. Y. Guo and A. Guadalupe, *Chem. Commun.*, 315 (1999).
138. EN 13727 : 2003 *Chemical Disinfectants and Antiseptics. Quantitative Suspension Test for the Evaluation of Bactericidal Activity of Chemical Disinfectants for Instruments Used in the Medical Area*, European Committee for Standardization, Brussels (2003).
139. EN 13624 : 2003 *Chemical Disinfectants and Antiseptics. Quantitative Suspension Test for the Evaluation of Fungicidal Activity for Instruments Used in the Medical Area*, European Committee for Standardization, Brussels (2003).
140. D. K. Tiwari, J. Behari1, and P. Sen, *Curr. Sci.*, **95**, No. 5, 647 (2008).
141. Yu. A. Krutyakov, A. A. Kudrinskii, A. Yu. Olenin, and G. V. Lisichkin, *Usp. Khim.*, **77**, No. 3, 242 (2008).
142. M. Kawashita, S. Toda, H.-M. Kim, et al., *J. Biomed. Mater. Res. A*, **66**, No. 2, 266 (2003).
143. G. Bugla-Płoskońska, A. Leszkiewicz, B. Borak, et al., *Int. J. Antimicrob. Agents*, **29**, No. 6, 746 (2007).